Available online at www.sciencedirect.com
ScienceDirect
Journal of Hazardous Materials 150 (2008) 53–61
Journal of Hazardous Materials
www.elsevier.com/locate/jhazmat

Decomposition kinetics of ammonia in gaseous stream by a nanoscale copper-cerium bimetallic catalyst

Chang-Mao Hung *

Department of Industry Engineering and Management, Yung-Ta Institute of Technology and Commerce, 316 Chung-shan Road, Linlo, Pingtung 909, Taiwan

Received 16 January 2006; received in revised form 12 January 2007; accepted 17 April 2007
Available online 20 April 2007

Abstract

This study performance is to examine the kinetics over nanoscale copper-cerium bimetallic catalyst under selective catalytic oxidation (SCO) of ammonia to N_2 in a tubular fixed-bed reactor (TFBR) at temperatures from 150 to 400 °C in the presence of oxygen. The nanoscale copper-cerium bimetallic catalyst was prepared by co-precipitation with $Cu(NO_3)_2$ and $Ce(NO_3)_3$ at molar ratio of 6:4. Experimental results showed that the catalyst with transmission electron microscopy (TEM) revealed that copper and cerium are well dispersed and catalyst in the form of nanometer-sized particles. Moreover, the kinetic behavior of NH_3 oxidation with catalysis can be accounted by using the rate expression of the Langmuir–Hinshelwood type kinetic model. Kinetic parameters are also developed on the basis of the differential reactor data. Also, experimental results are compared with those of the model predicted.

Keywords: Selective catalytic oxidation (SCO); Tubular fixed-bed reactor (TFBR); Ammonia; Nanoscale copper-cerium bimetallic catalyst; Kinetic

1. Introduction

Ammonia (NH_3) is widely found in industrial processes and it is a valuable chemical product for using with a variety of purposes and its can be eliminated in several ways, including ammonium nitrate production industry, livestock feedlots, urea manufacture plants, nitrogen fertilizer application industry, fossil fuel combustion or petroleum refineries, and refrigeration industry, which are either toxic inorganic gaseous and its pungent malodorous component under ambient conditions or have the potential harmful effects on the public [1–4]. It is also one of the control lists of the EPA, Taiwan. Moreover, conventional biological, physical, and chemical treatment processes, such as biofilters [5,6], stripping [7], water scrubbing [8], post-combustion control technologies [9], microwave-plasma discharge [10], electrochemical oxidation [11], and activated carbon fibers on soot adsorption [12,13], only make a phase transformation and may yield a contaminated sludge and/or an adsorbent, both needing for further disposal, and their maintenance or operation costs are high by physical and/or chemical methods. Therefore, the removal, control, and prevention of ammonia emission from air and waste streams are important. This discharge presents a challenging task because environmental laws and regulations regarding safe discharge are becoming increasingly stringent is a major concern.

More recently, catalytic oxidation has been known to enhance the possibilities of the advanced oxidation processes technology through the use of dedicated catalysts, which can potentially promote oxidation in shorter reaction times under milder operating conditions. The selective catalytic oxidation (SCO) for ammonia-containing stream to molecular nitrogen and water is one way to solve ammonia pollution problems [14–19]. There are some reports about catalytic oxidation of ammonia that can occur, and these are as follows:

$$N_2 + 3H_2 \rightarrow 2NH_3 \quad (1)$$

$$4NH_3 + 3O_2 \rightarrow 2N_2 + 6H_2O \quad (2)$$

$$2NH_3 + 2O_2 \rightarrow N_2O + 3H_2O \quad (3)$$

$$4NH_3 + 5O_2 \rightarrow 4NO + 6H_2O \quad (4)$$

There are not many types of catalysts that have been used for oxidation of ammonia in gaseous phase. For example, Amblard et al. [3] have demonstrated excellent selective conversion of

* Tel.: +886 8 7233733x508; fax: +886 8 7228046.
E-mail address: hungcm1031@gmail.com.

0304-3894/$ – see front matter © 2007 Elsevier B.V. All rights reserved.
doi:10.1016/j.jhazmat.2007.04.044

ammonia to nitrogen (>90%) by γ-Al_2O_3-supported Ni in selective catalytic oxidation processes. Furthermore, Wang et al. [15], who developed Ni-based catalysts for fuel gas oxidation from biomass gasification, found fresh Ni-based catalysts to be more active at lower temperature for the decomposition process of ammonia, and the partial pressure of hydrogen in the flue gas was a key factor to model ammonia oxidation. Liang [18] studied ammonia oxidation in a fixed-bed microreactor in the temperature range of 600–750 °C at GHSV = 1800–3600 h^{-1}. He observed that the conversion of ammonia reached 98.7 and 99.8% on nitrided MoN*x*/α-Al_2O_3 and NiMoN*y*/α-Al_2O_3 catalysts, respectively. Olofsson et al. [19] have demonstrated that excellent catalytic conversion of ammonia for nitrogen formation and by γ-Al_2O_3-supported Pt/CuO in selective catalytic oxidation processes. Among these, Schmidt-Szałowski [14] also published a paper covering a hypothetical model to explain the effect, the activity, and the selectivity in ammonia oxidation of the cobalt oxide catalyst's macrostructure on its properties.

As concerns reaction kinetic model, Lou [20] used a catalyst composed of Pt, Ni and Cr alloy of foam type to study the kinetics of catalytic incineration of butanone and toluene. He found that the Mars and van Krevelen model was suitable to describe the catalytic incineration of those volatile organic compounds (VOCs). Lou [21] used a Pt/Al_2O_3 alloy catalyst to study the kinetics of catalytic incineration of trichloromethane. He adopted power-rate law kinetics and found that the reaction was first-order in trichloromethane concentration and the activation energy was 16.2 kcal/mol. Lou [22] also used a 0.05% Pt/Ni/Cr alloy catalyst to study the kinetics of catalytic incineration of trichloromethane. He found that the Mars and van Krevelen model was suitable to describe the catalytic incineration of these VOCs. Gangwal [23] used a 0.1% Pt, 3% Ni/γ-Al_2O_3 catalyst to study the kinetics of deep catalytic oxidation with *n*-hexane and benzene. They found that the Mars and van Krevelen model was favorable to explain the catalytic combustion of a binary mixture at temperature ranging from 160 to 360 °C. Nitrogen compounds have been shown the similar manner, which were reversible inhibitors to the catalyst [24]. However, the kinetic studies of catalytic oxidation of NH_3 on metal composite catalysts have not been thoroughly investigated.

In this study, we investigate the nature of the adsorbed species formed on the catalyst surface using an interpretation of the kinetic data. Various kinetic models, including the power-rate law, the Mars and van Krevelen model, and the Langmuir–Hinshelwood model were evaluated in driving the rate expression for NH_3 oxidation. Hence, we sought to study the activity of the nanoscale copper-cerium bimetallic catalyst on oxidation of ammonia at various parameters and the kinetic behavior of ammonia removal in the effluent stream. Our results can provide valuable information for designing and treating an ammonia-related system.

2. Materials and methods

In the preparation of the nanoscale copper-cerium bimetallic catalysts used in this study were prepared by co-precipitation of copper(II) nitrate (GR grade, Merck, Darmstadt, Germany), and cerium(III) nitrate (GR grade, Merck, Darmstadt, Germany) at molar ratio of 6:4. They were then was calcined at 500 °C in an air stream for 4 h. The resulting powder was made into tablets using acetic acid as a binder. The tablets were later reheated at 300 °C to burn the binder out of the nanoscale copper-cerium bimetallic tablets. They were then crushed and sieved into various particle sizes ranging between 0.25 and 0.15 mm for later use.

The experiments were carried out on a tubular fixed-bed flow quartz reactor (TFBR). Four flowing gases, namely NH_3, prepared the feeding mixture and the diluent's gas, helium, at the inlet of the reactor, each of them was independently controlled with a mass flow regulator. High purity dry air was used as the carrier gas and controlled with a mass flow meter (Sierra instrument Inc., USA) in the range of 8–13 L/min. The weight of catalysts is 1 g (empty bed volume approximately at 1.2 cm^3). An inert material of γ-Al_2O_3 spheres (a hydrophilic inert material) was used to increase the interfacial area in gas phase for better mass transfer of ammonia from air. Hence, the limitations of external mass transfer and inter-particle diffusion were negligible in this reactor. The reaction tube (length 300 mm and inner diameter 28 mm) was placed inside a split tube furnace; and the tube containing the catalyst was also placed inside a spilt tube furnace. Two thermocouples of type K (Omega, USA) and a diameter of 0.5 mm were mounted and equally spaced along the catalyst bed. The thermocouples were also connected to a PID controller (FP21, Shimaaen Co Ltd, Japan) to maintain a uniform temperature in the tube within ±0.5%. The feed gas (GHSV, 92,000 ml/h-g) was controlled at the concentration of 1000 ppm NH_3 under a GHSV of 92,000 ml/h-g and a concentration of O_2 of 4%. The catalyst's deactivation was not apparent during the tests. The reaction rate (r) of NH_3 is defined as follows:

$$r = \frac{F}{V} \cdot (C_{in} - C_{out}) = \left(\frac{F}{V}\right) \cdot C_{in} \cdot X \tag{5}$$

in which r is the reaction rate of NH_3 (mol ml^{-1} s^{-1}), F/V is the space velocity per second, C_{in} and C_{out} are the inlet and outlet concentration (mol ml^{-1}) of NH_3, X is the conversion of NH_3 (%).

To study the oxidation kinetics expressions involving surface interactions and competitive adsorption of NH_3 over nanoscale copper-cerium bimetallic catalyst with highly active, three kinetic models: power-rate law model, Mars and van Krevelen model, and Langmuir–Hinshelwood model were examined [25–27]. These approaches will be adopted in the next section in this paper. The following overall rate equations were found using the Langmuir–Hinshelwood model (Eqs (6) and (7)) and the Mars and van Krevelen model (Eqs (8)–(11)) to describe the oxidation of ammonia, respectively.

$$-r_i = \frac{kK_iC_iK_{oi}C_{oi}}{(1 + K_iC_i + K_{oi}C_{oi})^2} \tag{6}$$

Eq (6) can be simplified to a linear function:

$$\sqrt{\frac{C_i}{-r_i}} = \frac{1}{\sqrt{K'}} + \frac{K''}{\sqrt{K'}}C_i \tag{7}$$

where

$$K_1' = \frac{kK_iC_iK_{oi}}{(1+K_iC_i)^2}, \quad K_1'' = \frac{K_{oi}}{1+K_iC_i},$$

$$K_2' = \frac{kK_iC_i\sqrt{K_{oi}}}{(1+K_iC_i)^2}, \quad K_2'' = \frac{\sqrt{K_{oi}}}{1+K_iC_i}$$

Moreover, the Langmuir–Hinshelwood model represents reactions in which the NH_3 can only adsorb chemically onto specific sites of the nanoscale copper-cerium bimetallic catalyst, each site can only adsorb unimolecular or atom and the adsorption is limited to a monolayer. Furthermore, Mars and van Krevelen reaction is adopted and shows the following sequences:

$$NH_3 + \text{oxidized catalyst} \xrightarrow{K_i} \text{reduced catalyst} + \text{products} \quad (8)$$

$$O_2 + \text{reduced catalyst} \xrightarrow{K_o} \text{oxidized catalyst} \quad (9)$$

In this mechanism, the above steps are assumed to be first-order in the respective gaseous species and then Mars and van Krevelen can derive the following rate expression from a classical kinetic treatment

$$-r_i = \frac{K_iC_iK_{oi}C_{oi}}{K_iC_i + \alpha_iK_{oi}C_{oi}} \quad (10)$$

Eq (10) can be simplified to a linear function:

$$\frac{1}{-r_i} = \frac{\alpha_i}{K_{oi}C_{oi}} + \frac{1}{K_iC_i} \quad (11)$$

where k, K_{oi}, K_i are constants. K_i is the surface reduction rate constant (s^{-1}), K_{oi} is the surface reoxidation rate constant (s^{-1}), C_i is the oxygen concentration, and C_{oi} is the NH_3 inlet concentration. When $K_{oi}\,C_{oi} \gg K_i\,C_i$ in Eq (6) and $K_i\,C_i \gg \alpha_i\,K_{oi}\,C_{oi}$ in Eq (10) two rate equations can be expressed as the power-rate law form; they will be discussed below. Accordingly, the Mars and van Krevelen mechanism reaction between adsorbed oxygen and an adsorbed reactant of catalytic oxidation over metal oxides is also a redox mechanism involving gas-phase and lattice oxygen as well as gas-phase oxygen.

Samples before and after reaction were injected automatically with a sampling valve into a gas chromatograph (Shimadzu GC-14A) equipped with a thermal conductivity detector. A stainless-steel column (Porapak Q 80/100 mesh) was used for separation and analysis of the concentrations of N_2O isothermally at 100 °C. NH_3 was injected automatically before and after the reaction with a sampling valve into a gas chromatograph (Shimadzu GC-14A) equipped with a TCD (Shimadzu, Kyoto, Japan). The signal areas were measured electronically with a data integrator (CR-6A, Shimadzu). The concentrations of NO, NO_2 and O_2 in the gas samples were measured by a portable flue gas analyzer (IMR3000, IMR, Germany), which was linked to the designed location for continuous monitoring during combustion. Gas samples with known concentrations of NH_3 were used for the calibration.

Transmission electron microscopy (TEM) (Philips CM-200 Twin, Netherlands) elucidated the morphology of the catalysts and yielded information on the distribution of copper-cerium species on the catalyst surface. UV–vis absorption spectra were performed with a photo spectrophotometer (MCPD-3000, OTSUKA Electronics, Osaka, Japan) for the solid sample. The measured reflectance is relative to a $BaSO_4$ standard.

3. Results and discussions

Table 1 lists the test conditions: the concentration of the single compound, the space velocity, and the operating temperature. The procedures consisted of experiments with a differential reaction. Differential reaction experiments were performed to investigate the various kinetic models and it was evaluated to derive the rate expression for the NH_3 oxidation.

Fig. 1 presents the surface morphological changes of nanoscale copper-cerium bimetallic catalyst elucidating using TEM to provide information on the fresh/aged catalyst surface structure. Fig. 1a indicates that nanoscale copper-cerium bimetallic exhibits more aggregation and crystalline than observed in Fig. 1b. These crystal phases may explain the high activity of the catalysts. Fig. 1b indicates that disaggregated and dispersed phases were formed when the surface of the catalyst was aged or when poisoning occurred because of plugging, implying that the porosity of the particles had changed. These crystal phases may be responsible for the high activity of the catalysts. These results also confirm that the dispersion phenomena of the nanoscale copper-cerium bimetallic catalyst increase the efficiency of removal of NH_3.

To gain further information on the state of copper-cerium species in these catalysts, the UV–vis spectroscopic studies are carried out and the spectra are shown in Fig. 2. Generally, two bands were observed for these copper-cerium catalysts at 330 and 600–800 nm. The band at 330 nm is attributed to the Cu^{2+}–O^{2-} electronic transition species. The band at 600–800 nm is assigned to the octahedrically coordinated Cu^{2+} in the literature [28]. The formation of these species is in good with Carvalho [28], who indicated the reductive effect of NH_3 on nanoscale copper-cerium catalyst. The band at 600–900 nm is also assigned to *d–d* transitions of Cu^{2+} situated in an octahedral environment with an O_h symmetry [29]. In addition, bulk CeO_2 also shows strong absorption in this region. We thus prefer to assign the band at 340–350 nm to the bulk-like CeO_2 species. CeO_2 in a copper-cerium bimetallic catalyst may be assumed to promote the generation of the active phase of CuO under the conditions of NH_3 oxidation.

Table 1
Experimental conditions of test gas

Reaction type	Space velocity (1/h)	Residence period (s)	NH_3 concentration (ppm)	Temperature (°C)	Oxygen content (%)	Temperature rises (D*T*)
differential	92,000	0.04	1000	150–400	4	<1

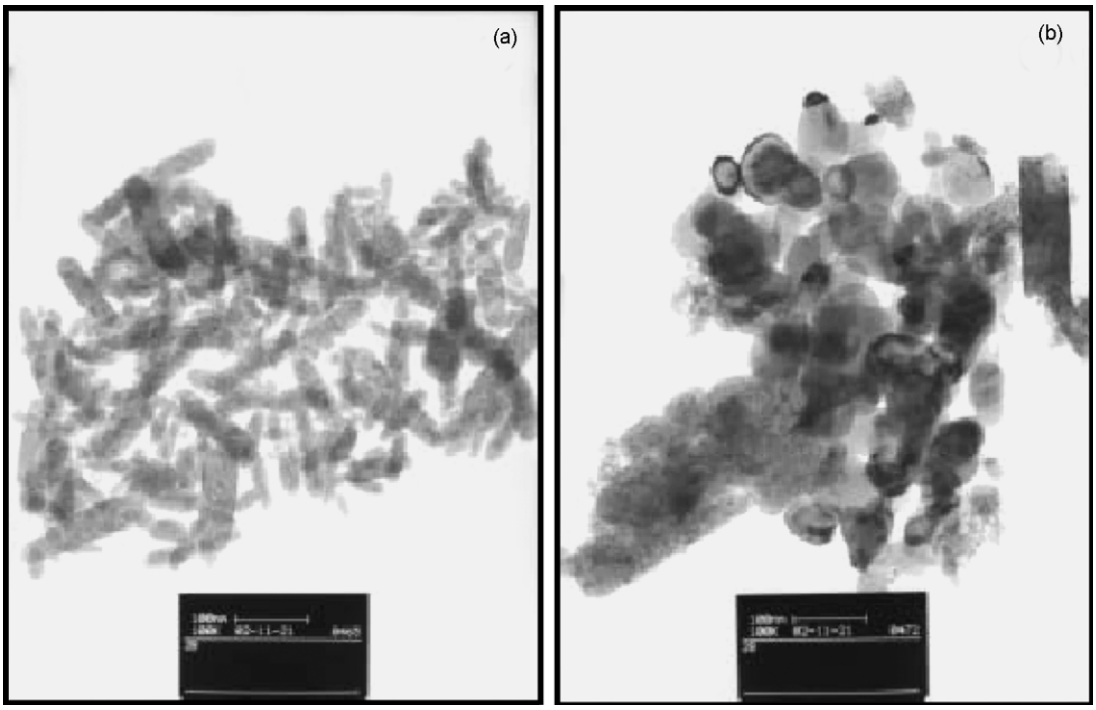

Fig. 1. TEM photograph of (a) fresh and (b) after activity test nanoscale copper-cerium bimetallic catalyst. Test conditions: 1000 ppm NH_3 in He, O_2 = 4%, GHSV = 92,000 ml/h-g.

The measured rates of oxidation of NH_3 in air stream were correlated first using the empirical power rate law kinetics. Then the dependence of the rate of NH_3 oxidation on the concentration of NH_3 and oxygen was tested using the following power-rate law equation:

$$-r_i = kC_i^n C_{O_2}^m \tag{12}$$

in which k is the reaction constant, and m and n are reaction orders. Since $C_{O_2} > C_i$ in most systems of catalyst incineration, the term can be assumed as a constant. Table 2 shows the reaction rates of catalytic incineration of NH_3 for the fixed O_2 concentration, which were calculated from Eq (5). Therefore, Fig. 3 plots $-\ln(-r_i)$ versus $-\ln C_i$ for NH_3 oxidation at several temperatures. The reaction order of C_i can be obtained from the slope of each line in Fig. 4. The linearity of plots results reveals a hypothesis of approximately first-order kinetic with changing from 0.55 to 0.94 in the NH_3 oxidation. In addition, the reaction constant k can be obtained from the intercept of each line in Fig. 3. Next, plotting the $\ln K$ versus T^{-1}, as shown in Fig. 4, attains a straight line. Via its intercept and its slope, the values of the pre-exponential factor [$A = 2.02 \times 10^8\ s^{-1}$] and the

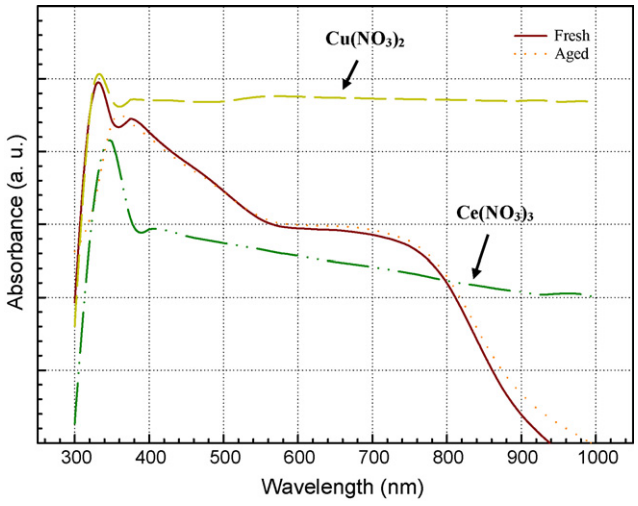

Fig. 2. UV–vis absorption spectra of (a) fresh and (b) after activity test nanoscale copper-cerium bimetallic catalyst. Test conditions: 1000 ppm NH_3 in He, O_2 = 4%, GHSV = 92,000 ml/h-g.

Table 2
The reaction rates of catalytic incineration of ammonia of fixed O_2 concentration at 4%

Inlet temperature (°C)	Inlet NH_3 concentration (10^{-8} mol/cm^3)	Reaction rate (10^{-7} mol/cm^3/s)
150	2.04	1.17
	2.45	1.40
	3.27	1.86
	4.08	2.31
200	2.04	1.41
	2.45	1.64
	3.27	2.15
	4.08	2.64
250	2.04	2.25
	2.45	2.45
	3.27	2.88
	4.08	3.31
300	2.04	2.69
	2.45	3.03
	3.27	3.55
	4.08	4.07

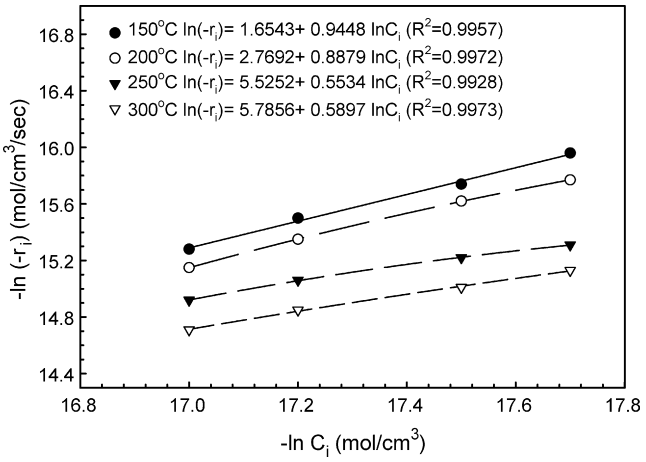

Fig. 3. Linear fitting of NH_3 kinetic data for the power-rate law.

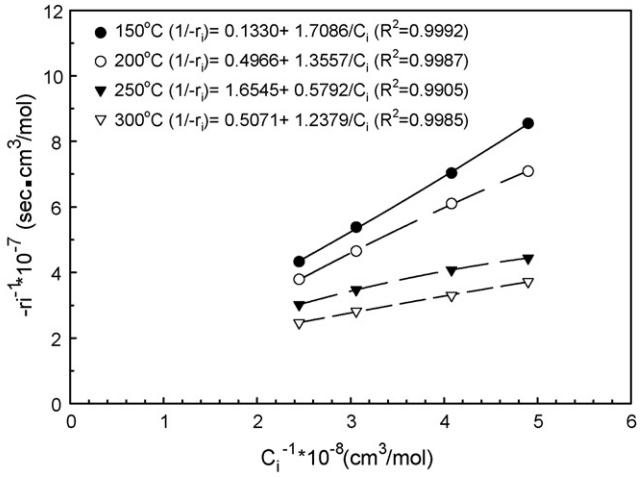

Fig. 5. Linear fitting of NH_3 kinetic data for the Mars and van Krevelen model.

apparent activation energy of NH_3 oxidation ($E_a = 62.1$ kJ/mol) were calculated from Arrhenius relationships. It is suggested that the power-rate law model was not feasible for the oxidation of ammonia over the nanoscale copper-cerium bimetallic catalyst since the R^2 value ($R^2 = 0.9285$) for the rate constants fitting is relatively low.

The dependence of the rate of NH_3 oxidation on the concentration of NH_3 and oxygen was tested using the following Mars and van Krevelen classical kinetic model of oxidation reaction with competition for surface adsorbed oxygen was assumed. In this study, Fig. 5 plots r_i^{-1} versus C_i^{-1} for NH_3 oxidation at several temperatures. The reaction order of C_i^{-1} can be obtained in this manner from the slope of each line in Fig. 5. The values of K_i and K_{oi} can be calculated from Eq (11) and the linearity of plots results reveals a reaction with changing from 0.50 to 1.65 in the NH_3 oxidation. In addition, the reaction constant k can be obtained from the intercept of each line in Fig. 5. Next, plotting the ln K versus T^{-1}, as shown in Fig. 6, attains a straight line. Via its intercept and its slope, the values of the pre-exponential factor [$A_i = 24.0\ s^{-1}$; $A_{oi} = 2 \times 10^2\ s^{-1}$] and the apparent activation energy of NH_3 oxidation, E_i, 12.2 kJ/mol and the apparent activation energy of NH_3 oxidation, E_{oi}, 24.1 kJ/mol were calculated from Arrhenius relationships, respectively. If the ammonia react with the gas phase or adsorbed on different catalyst sites, a Mars and van Krevelen type kinetic model will be observed, and mutual inhibition is through competition for adsorbed oxygen. Consequently, it is suggested that the Mars and van Krevelen model was not feasible for the oxidation of ammonia over the nanoscale copper-cerium bimetallic catalysts since the R^2 value ($R^2 = 0.8213$ and 0.9151, respectively) for the rate constants fitting is relatively low.

The dependence of the rate of NH_3 oxidation on the concentration of NH_3 and oxygen was tested using the following Langmuir–Hinshelwood model with reaction between oxygen and ammonia adsorbed over the surface sites. In this study, Fig. 7 plots $(C_i/-r_i)^{1/2}$ versus C_i for NH_3 oxidation at several temperatures. The R^2 value for various lines shows fairly good agreements. Table 3 shows the reaction rates of oxidation of NH_3 for fixed NH_3 concentration. In addition, the reaction constant K_1' and K_2'' can be obtained from Eq (7) and the results are also given in Table 4. Fig. 8 plots $(C_{oi}/-r_{oi})^{1/2}$ versus C_{oi} for

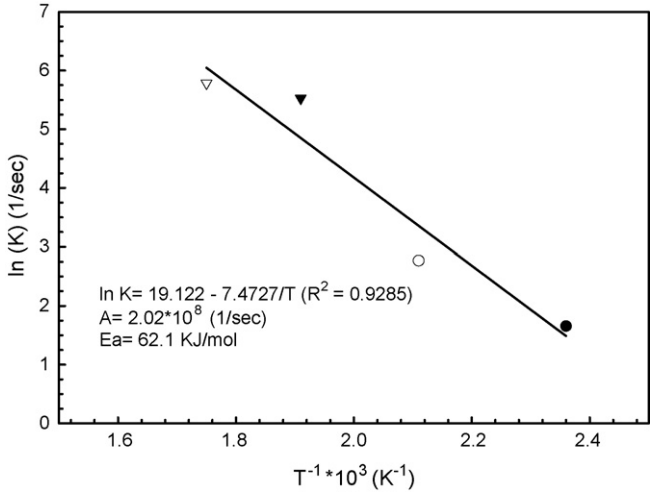

Fig. 4. Arrhenius equation fitting of NH_3 kinetic data for the power-rate law.

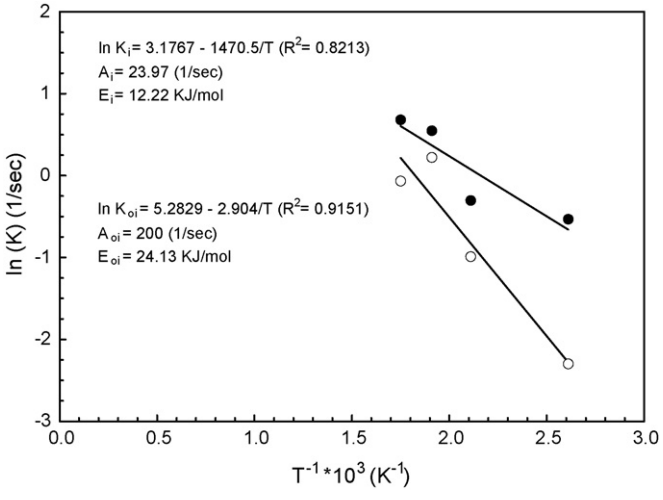

Fig. 6. Arrhenius equation fitting of NH_3 kinetic data for the Mars and van Krevelen model.

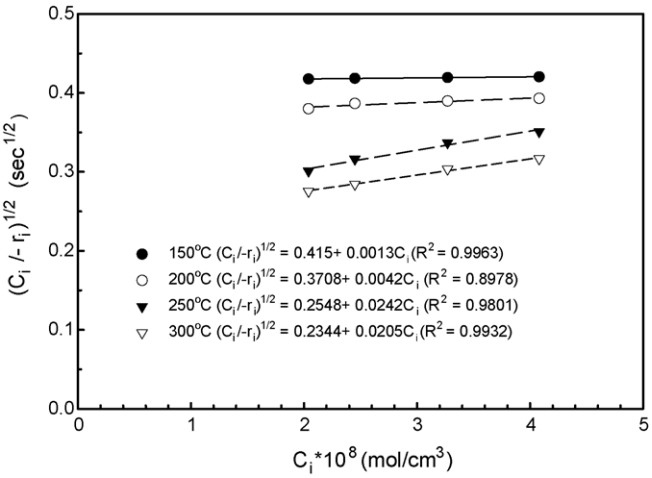

Fig. 7. Calculating K_1' and K_2'' by linear fitting of NH_3 kinetic data for the Langmuir–Hinshelwood model.

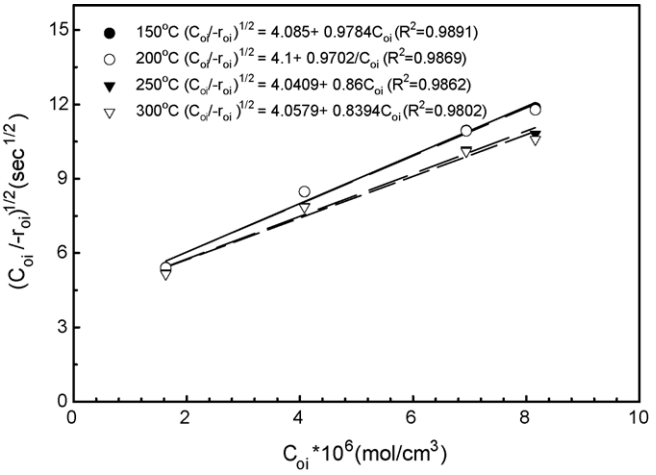

Fig. 8. Calculating K_1' and K_2'' by linear fitting of NH_3 kinetic data for the Langmuir–Hinshelwood model involving molecular oxygen adsorption.

Table 3
The reaction rates of catalytic incineration of ammonia fixed NH_3 concentration at 1000 ppm

Inlet temperature (°C)	Inlet O_2 concentration (10^{-6} mol/cm^3/s)	Reaction rate (10^{-8} mol/cm^3/s)
150	1.63	5.55
	4.08	5.68
	6.94	5.78
	8.16	5.79
200	1.63	5.58
	4.08	5.67
	6.94	5.80
	8.16	5.87
250	1.63	6.01
	4.08	6.55
	6.94	6.71
	8.16	7.00
300	1.63	6.13
	4.08	6.59
	6.94	6.79
	8.16	7.27

Table 4
The composite rate constants of the Langmuir–Hinshelwood model for the reduction of ammonia

	Inlet temperature (°C)			
	150	200	250	300
(1) Fixed O_2 concentration				
K'	5.8	7.9	15.4	18.2
$K'' \times 10^{-2}$	0.3	1.1	9.5	8.8
(2) Fixed NH_3 concentration				
(a) Molecular oxygen adsorption				
K_1'	0.05	0.05	0.06	0.06
K_1''	0.23	0.23	0.21	0.20
(b) Atomic oxygen adsorption				
$K_2' \times 10^{-5}$	9.34	10.6	9.91	9.79
K_2''	0.37	0.45	0.36	0.34

NH_3 oxidation at several temperatures and its involving molecular oxygen adsorption. The reaction order of C_{oi} can be obtained from the slope of each line in Fig. 8. The linearity of plots results reveals an approximately first-order reaction changing from 0.83 to 0.98 in the NH_3 oxidation. Via its intercept and its slope, the values of the pre-exponential factor [$A = 1.2 \times 10^{-7}$ s^{-1}] and the apparent activation energy of NH_3 oxidation ($E_a = 27.8$ kJ/mol) were calculated from Arrhenius relationships in Fig. 9. Fig. 10 plots $((C_{oi})^{1/2}/-r_{oi})^{1/2}$ versus $C_{oi}^{1/2}$ for NH_3 oxidation at several temperatures and its involving atomic oxygen adsorption. Accordingly, ammonia reacts from gas phase with adsorption oxygen atomic and molecular oxygen. If the surface reaction is much slower than the adsorption processes, then equilibrium adsorption will occur and a Langmuir–Hinshelwood type is observed [30]. The reaction order of C_{oi} can be obtained from the slope of each line in Fig. 10. Via its intercept and its slope, the values of the pre-exponential factor [$A = 0.36$ s^{-1}] and the apparent activation energy of NH_3 oxidation ($E_a = 40.7$ kJ/mol) were calculated from Arrhenius relationships in Fig. 11. The linearity of

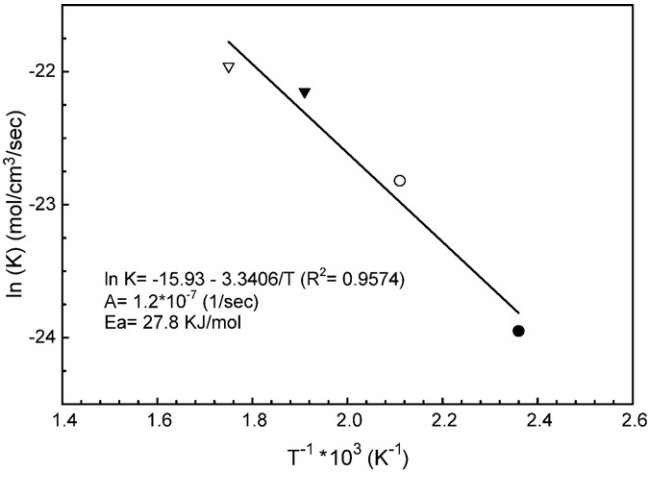

Fig. 9. Arrhenius equation fitting of NH_3 kinetic data for the Langmuir–Hinshelwood model involving molecular oxygen adsorption.

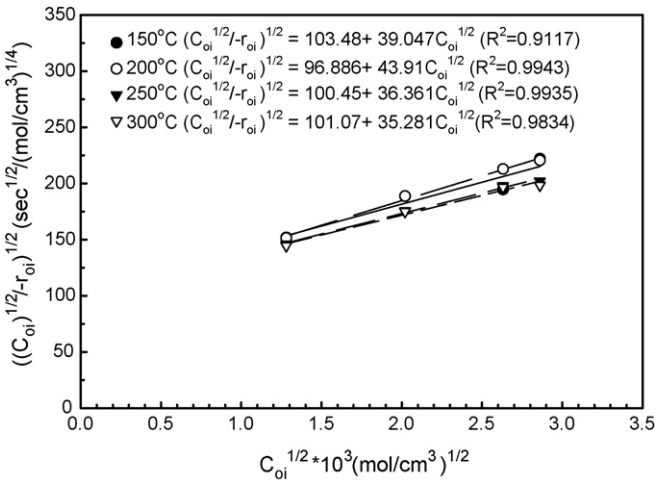

Fig. 10. Calculating K_1' and K_2'' by linear fitting of NH_3 kinetic data for the Langmuir–Hinshelwood model involving atomic oxygen adsorption.

Table 5
The reaction rates constants and adsorption equilibrium constants of the Langmuir–Hinshelwood model for the reduction of ammonia

Inlet temperature (°C)	Molecular oxygen adsorption k (10^9 mol/cm^3/s)	Atomic oxygen adsorption k (10^8 mol/cm^3/s)
150	3.691	12.67
200	1.741	4.731
250	0.240	4.125
300	0.289	6.040

plots results reveals an approximately first-order reaction in the NH_3 oxidation. Hence, the linearity of plots results suggests the fitness of the Langmuir–Hinshelwood mechanisms for ammonia. Arrhenius relationships and plots for the corresponding k values for ammonia are shown in Figs. 9 and 11, respectively. Table 5 shows the reaction rates and adsorption equilibrium of oxidation of NH_3 for fixed NH_3 concentration. As a result, it is suggested that the Langmuir–Hinshelwood type kinetic model

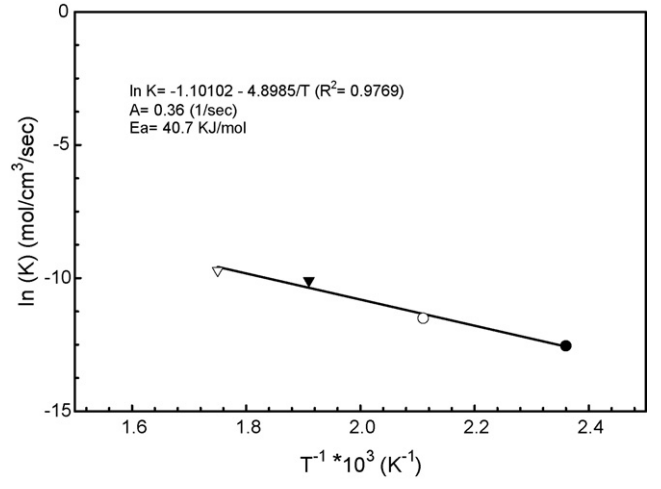

Fig. 11. Arrhenius equation fitting of NH_3 kinetic data for the Langmuir–Hinshelwood model involving atomic oxygen adsorption.

involving molecular oxygen and atomic oxygen adsorptive reactivity and competition adsorption surface sites remarkably were feasible for the oxidation of ammonia over the nanoscale copper-cerium bimetallic catalysts since the R^2 value (R^2 = 0.9574 and 0.9769, respectively) for the rate constants fitting is relatively high. Thus, the proposed kinetic models proved to predict reaction mechanism and rates satisfactorily. The result is similar to that described in relevant literature [31–35].

Results showed that the kinetic behavior of NH_3 oxidation with catalysis could be explained by using the rate model of Langmuir–Hinshelwood. Regarding the rate expressions for the oxidation of NH_3 catalyzed by nanoscale copper-cerium bimetallic catalyst, the kinetic parameters such as K and E_a were obtained by the linear regression method, we can substituted into Arrhenius equation and an equation of the theoretical values of conversion at various reaction temperatures is

$$X = 1 - \exp[-2 \times 10^2 \cdot \exp\left(\frac{-24.13}{RT}\right) \cdot \tau] \quad (13)$$

in which X is the conversion, R is the gas constant, T is the temperature of the reactor and τ is the residence period. The relation between the residence period for actual entering conditions and at reactor conditions is given by

$$\tau = \tau_0 \cdot \left(\frac{T}{T_0}\right) \quad (14)$$

in which τ_0 and T_0 are the residence period and the absolute temperature of the stream entering the reactor, respectively. In most cases, our residence period was based on the feed for actual entering conditions.

Fig. 12 compares predicted and experimental conversions obtained by and isothermal differential fixed-bed reactor at temperatures ranging from 150 to 400 °C. This figure reveals that the model accurately predicts the NH_3 conversion and

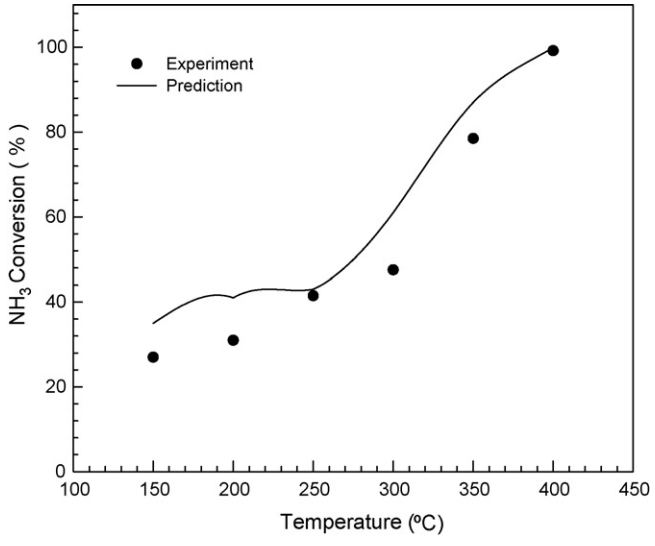

Fig. 12. Comparison of experimental data (symbols) and computed values (solid lines) from conversions of the rate equation at different temperatures of NH_3 by Langmuir–Hinshelwood type model. Test conditions: 1000 ppm NH_3 in He, O_2 = 4%, GHSV = 92,000 ml/h-g.

the conversion of ammonia increased greatly from 38 to 99% (150–400 °C). The removal efficiency increases with increasing temperature and decreasing residence period. The deviation is enhanced, particularly in the region (250–400 °C) of a high concentration of NH_3 (1000 ppm). In this case, the temperature increase was measured indicating that the temperature effects of NH_3 in high concentration also slightly promoted the conversion of NH_3 oxidation; thus, conversions were slightly greater than the predicted values. This model is appropriate for oxygen presence conditions and high concentration of NH_3.

4. Conclusions

The catalytic oxidation of ammonia over the nanoscale copper-cerium bimetallic catalyst was found to lead to more effective ammonia removal containing air stream and selective catalytic process was found to be more effective at lower temperatures. A kinetic rate expression was developed to describe the data over the range of conditions investigated. Moreover, correlation equations in the form of Arrhenius's law are derived from experimental data to predict the destruction efficiencies of ammonia from the temperatures and residence period in a catalytic process. A Langmuir–Hinshelwood model incorporating a first-order reaction appears to adequately represent the NH_3 oxidation, which shows fairly good agreements with experimental data. The apparent activation energy is 27.8 kJ/mol. This kinetic model is appropriate for oxygen presence and high concentrations of NH_3. In this work, we use the catalytic oxidation showing a promise in the treatment of highly concentrated ammonia stream, thereby helping industrial plants meet the discharge regulations.

Acknowledgments

The author would like to thank the National Science Council of the Republic of China, Taiwan for financially supporting this research. The author thanks Mr. S.F. Yang in the Institute of Environmental Engineering at National Sun Yat-Sen University for his support and discussions.

References

[1] W. Mojtahedi, J. Abbasian, Catalytic decomposition of ammonia in a fuel gas at high temperature and pressure, Fuel 74 (1995) 1698–1703.
[2] T. Kurvits, T. Marta, Agricultural NH_3 and NO_x emissions in Canada, Environ. Pollut. 102 (1998) 187–194.
[3] M. Amblard, R. Burch, B.W.L. Southward, A study of the mechanism of selective conversion of ammonia to nitrogen on Ni/γ-Al_2O_3 under strongly oxidizing conditions, Catal. Today 59 (2000) 365–371.
[4] J.C. Lou, C.M. Hung, S.F. Yang, Selective catalytic oxidation of ammonia over copper-cerium composite catalyst, J. Air Waste Manage. Assoc. 54 (2004) 68–76.
[5] N.J. Kim, M. Hirai, M. Shoda, Comparison of organic and inorganic packing materials in the removal of ammonia gas in biofilters, J. Hazard. Mater. B72 (2000) 77–90.
[6] Y.C. Chung, C. Huang, C.H. Liu, H. Bai, Biotreatment of hydrogen sulfide- and ammonia-containing waste gases by fluidized bed bioreactor, J. Air Waste Manage. Assoc. 51 (2001) 163–172.
[7] T.L. Huang, K.R. Cliffe, J.M. Macinnes, The removal of ammonia from water by a hydrophobic catalyst, Environ. Sci. Technol. 34 (2000) 4804–4809.
[8] R. Burch, B.W.L. Southward, The nature of the active metal surface of catalysts for the clean combustion of biogas containing ammonia, J. Catal. 198 (2001) 286–295.
[9] T. Hasegawa, M. Sato, Study of ammonia removal from coal-gasified fuel, Combust. Flame 114 (1998) 246–258.
[10] M.A. Wójtowicz, F.P. Miknis, R.W. Grimes, W.W. Smith, M.A. Serio, Control of nitric oxide, nitrous oxide, and ammonia emissions using microwave plasmas, J. Hazard. Mater. 74 (2000) 81–89.
[11] A.C.A. de Vooys, M.T.M. Koper, R.A. van Santen, J.A.R. van Veen, The role of adsorbates in the electrochemical oxidation of ammonia on noble and transition metal electrodes, J. Electroanal. Chem. 506 (2001) 127–137.
[12] C.L. Mangun, R.D. Braatz, J. Economy, A.J. Hall, Fixed bed adsorption of acetone and ammonia onto oxidized activated carbon fibers, Ind. Eng. Chem. Res. 38 (1999) 3499–3504.
[13] A.H. Muenter, B.G. Koehler, Adsorption of ammonia on soot at low temperatures, J. Phys. Chem. A 104 (2000) 8527–8534.
[14] K. Schmidt-Szałowski, K. Krawczyk, J. Petryk, The properties of cobalt oxide catalyst for ammonia oxidation, Appl. Catal. A: General 175 (1998) 147–157.
[15] W. Wang, N. Padban, Z. Ye, A. Andersson, I. Bjerle, Kinetic of ammonia decomposition in hot gas cleaning, Ind. Eng. Chem. Res. 38 (1999) 4175–4182.
[16] T. Curtin, F.O. Regan, C. Deconinck, N. Knűttle, B.K. Hodnett, The catalytic oxidation of ammonia: influence of water and sulfur on selectivity to nitrogen over promoted copper oxide/alumina catalysts, Catal. Today 55 (2000) 189–195.
[17] L. Lietti, G. Ramis, G. Busca, F. Bregani, P. Forzatti, Characterization and reactivity of MoO_3/SiO_2 catalysts in the selective catalytic oxidation of ammonia to N_2, Catal. Today 61 (2000) 187–195.
[18] C. Liang, W. Li, Z. Wei, Q. Xin, C. Li, Catalytic decomposition of ammonia over nitrided MoNx/α-Al_2O_3 and NiMoNy/α-Al_2O_3 catalysts, Ind. Eng. Chem. Res. 39 (2000) 3694–3697.
[19] G. Olofsson, A. Hinz, A. Andersson, A transient response study of the selective catalytic oxidation of ammonia to nitrogen on Pt/CuO/Al_2O_3, Chem. Eng. Sci. 59 (2004) 4113–4123.
[20] J.C. Lou, C.L. Chen, Destruction of butanone and toluene with catalytic incineration, Hazard. Waste Hazard. Mater. 12 (1995) 37–49.
[21] J.C. Lou, S.S. Lee, Destruction of trichloromethane with catalytic oxidation, Appl. Catal. B: Environ. 12 (1997) 111–123.
[22] J.C. Lou, S.S. Lee, Kinetics study of trichloromethane with catalysis, J. Chin. Inst. Environ. Eng. 5 (1995) 301–307.
[23] S.K. Gangwal, M.E. Mullins, J.J. Spivey, P.R. Caffrey, Kinetics and selectivity of deep catalytic oxidation of *n*-hexane and benzene, Appl. Catal. 36 (1988) 231–247.
[24] J.T. Richardson, Principles of Catalyst Development, Plenum Press, New York, 1989.
[25] C.N. Satterfield, Heterogeneous Catalysis in Industrial Practice, McGraw-Hill, New York, 1991.
[26] P. Mars, D.W. van Krevelen, Oxidation carried out by means of vanadium oxide catalysts, Chem. Eng. Sci. 3 (1954) 41–59.
[27] T.K. Tseng, H. Chu, T.H. Ko, L.K. Chaung, The kinetic of the catalytic decomposition of methyl isobutyl ketone over a Pt/γ-Al_2O_3 catalyst, Chemosphere 61 (2005) 469–477.
[28] M.C.N.A. Carvalho, F.B. Passos, M. Schmal, The behavior of Cu/ZSM-5 in the oxide and reduced form in the presence of NO and methanol, Appl. Catal. A: General 193 (2000) 265–276.
[29] L. Chen, T. Horiuchi, T. Osaki, T. Mori, Catalytic selective reduction of NO with propylene over Cu-Al_2O_3 catalysts: influence of catalyst preparation method, Appl. Catal. B: Environ. 23 (1999) 259–269.
[30] A.A. Barresi, G. Baldi, Deep catalytic oxidation kinetics of benzene-ethenylbenzene mixtures, Chem. Eng. Sci. 47 (1992) 1943–1953.
[31] G. Papapolymerou, V. Bontozoglou, Decomposition of NH_3 on Pd and Ir comparison with Pt and Rh, J. Mol. Catal. A: Chem. 120 (1997) 165–171.

[32] M. Trombetta, G. Ramis, G. Busca, B. Montanari, A. Vaccari, Ammonia adsorption and oxidation on Cu/Mg/Al mixed oxide catalysts prepared via hydrotalcite-type precursors, Langmuir 13 (1997) 4628–4637.
[33] Y.W. Budhi, A. Jaree, J.H.B.J. Hoebink, J.C. Schouten, Simulation of reverse flow operation for manipulation of catalyst surface coverage in the selective oxidation of ammonia, Chem. Eng. Sci. 59 (2004) 4125–4135.
[34] A. Boisen, S. Dahl, J.K. Nørskov, C.H. Christensen, Why the optimal ammonia synthesis catalyst is not the optimal ammonia decomposition catalyst, J. Catal. 230 (2005) 309–312.
[35] L. Hannevold, O. Nilsen, A. Kjekshus, H. Fjellvåg, Reconstruction of platinum-rhodium catalysts during oxidation of ammonia, Appl. Catal. A: General 284 (2005) 163–176.